The Pharmaceutical and Chemical Journal, 2023, 10(5):98-112

Available online www.tpcj.org

Research Article

ISSN: 2349-7092
CODEN(USA): PCJHBA

Bioaccumulation and Oxidative Stress of Aluminum Oxide Nanoparticles in some Brain Regions of Male Albino Rats

[1]Gamal M Morsy, [3]Afaf Ismail Mohamed El amen, [3]Rami B. Kassab, [2]Omar A. Ahmed-Farid, [3]Mona Abdel-Rahman

[1]Department of Zoology, Faculty of Science, Cairo University, Giza, Egypt.
[2]Physiology Department, Egyptian Drug Authority, Giza, Egypt.
[3]Zoology and Entomology Department, Faculty of Science, Helwan University, Ain Helwan, 11795, Cairo, Egypt.

Abstract This study aimed to assess oxidative stress in the hippocampus, cortex, striatum, and midbrain of male rats in response to Al ions accumulated in these areas following nasal instillation of nano-alumina (Al_2O_3NPs) every other day. Rats were divided into groups I and II. The first group was administered deionized water (control), whereas the second group was instilled with a subacute dose of 0.94 mg/kg for 3, 7, and 14 days. The present findings show that the accumulation of Al ions and malondialdehyde (MDA) levels in all investigated brain areas of Group II were significantly higher than those of Group I at all corresponding periods, whereas glutathione (GSH) levels were significantly decreased. The experimental periods exhibited significant direct relationships with Al ions and MDA levels in the hippocampus, cortex, striatum, and midbrain of Group II, with considerable positive correlation coefficients, whereas the concentrations of GSH showed a significant inverse relationship and were associated with marked negative correlation coefficients. Additionally, in group II, there were strong inverse relationships between Al ions accumulated in the brain and their GSH content, with significant negative correlation coefficients, whereas the levels of MDA were positively and significantly correlated, with a positive and considerable correlation coefficient. In conclusion, the current findings affirm that repeated dosages of Al_2O_3NPs have a high tendency to accumulate in brain regions with a high potential to induce oxidative stress.

Keywords Nano-alumina, bioaccumulation, brain areas, oxidative stress, glutathione, malondialdehyde.

1. Introduction

Nanomaterials with grain sizes of one billionth of a meter [1] exhibit a variety of specific features owing to their unique structure. Consequently, they have a wide range of applications [2, 3, 4, 5]. Nanomaterial particles are commonly used as nanoparticles (NPs) in various sectors, including catalysis, ceramics, polymer modification, heat transfer fluids, wastewater treatment, and biological applications [6]. Nano-alumina has the unique ability to interact with cells and the surrounding environment in a manner that its larger biological counterparts cannot. This is primarily because of their extremely small size [7]. When nanoparticles are released into the environment, they can easily enter the cells through receptor-mediated endocytosis or passive diffusion. Once inside the cells, they interact with cellular proteins, lipids, and genomic DNA [8,9]. This leads to oxidative stress induced by Reactive Oxygen Species (ROS), which are the primary factors contributing to nanotoxicity [10,11]. Despite the antioxidant properties of some nanoparticles, such as gold, silver, copper, and iron, most of them are implicated in the generation of

intracellular ROS. This generation is dependent on factors such as cellular absorption of nanoparticles, intracellular responses, and release of metal ions [12–13]. Additionally, these nanoparticles are produced during various cellular signaling processes and play a crucial role in immune system defense mechanisms [14]. ROS can potentially damage important biological macromolecules including proteins, lipids, and DNA. This damage can have harmful effects on cellular organelles and cause mitochondrial dysfunction [15]. Moreover, excessive levels of ROS can cause various toxicological reactions, such as apoptosis, necrosis, hypertrophy, genotoxicity, inflammation, fibrosis, and even cancer. It also increases the production of proinflammatory cytokines and activates inflammatory cells such as macrophages, which further increases the production of ROS [16]. Owing to its unique characteristics such as small size, large specific surface area, and high reactivity, nano-alumina may act on the BBB and its related connective proteins under contact conditions to change its permeability and mediate central nerve injury. Additionally, nano-alumina has been identified as a significant factor in numerous neurodegenerative conditions, including Alzheimer's and Parkinson's diseases [17]. The initial occurrence of oxidative damage to nerve cells is the primary consequence of nanoparticle toxicity, resulting in detrimental effects [18]. Nano-alumina possesses unique characteristics such as compact size, expansive specific surface area, and heightened reactivity. When interacting with the blood-brain barrier (BBB) and its connected proteins, nano-alumina may potentially influence the permeability of the BBB and its associated connective proteins owing to these distinctive properties. This study aimed to evaluate the bioaccumulation of nanoalumina in the brain regions of rats (hippocampus, cortex, striatum, and midbrain) through subacute experimentation. Additionally, we investigated whether there was a correlation between the accumulation of Al ions and the experimental period, biomarker toxicity of malondialdehyde (MDA) as an oxidative stressor, and levels of glutathione (GSH) as a non-enzymatic antioxidant. This was achieved by subjecting rats to subacute nasal instillation with nano-alumina.

2. Materials and Methods

2.1 Experimental Animals and Chemicals

Adult male rats weighing 150±10 g was used as experimental models. The rats were acclimatized to laboratory conditions for seven days. The temperature range was 22°C to 24 °C, with a relative humidity of 30% to 35% and a 12-hour light/dark cycle. During the acclimatization period, the rats were provided with free access to a commercial pelleted diet and water. To maintain cleanliness, food debris and feces were removed from the cages, which were cleaned daily to ensure that the sawdust remained dry throughout the duration of the experiments. The experimental procedures were conducted in accordance with the international guidelines for the care and use of laboratory animals in scientific research. All experiments were performed under normal laboratory conditions at the Zoology Department, Faculty of Science, Helwan University, Cairo, Egypt.

The raw aluminum oxide nanoparticles (Al2O3NPs: primary particle size ≤ 13 nm, surface area 100±10 m^2/g) were purchased from Sigma-Aldrich (St. Louis, Missouri, USA; 99.98% purity).

2.2 Experimental Design

The current experiments were designed to study the bioaccumulation of Al_2O_3NPs and its potential oxidative stress in some brain areas (hippocampus, cortex, striatum, and midbrain) of rats during subacute experiments after intranasal instillation with Al_2O_3NPs. Thirty healthy male rats (N = 30) were allocated into two main groups, I and II, each comprising 15 rats. Group I were intranasally instilled with deionized water (control rats), whereas those of group II were intranasally instilled every other day for 14 days with LD5 of Al_2O_3NPs at 96 h (subacute dosages) equivalent to 0.96 g/kg b. wt.

2.3 Sampling

After 3, 7, and 14 days of installation, five rats were selected from each cage and euthanized in a humane manner through sudden decapitation. Subsequently, the brains were immediately removed from their skulls, swollen, and cooled. Filter paper was then used to quickly dry the brain tissue. The dissection process was conducted on an ice-chilled glass plate, and four specific brain regions (the hippocampus, cortex, striatum, and midbrain) were separated

according to the method described by Glowinski et al. in 1966. Each brain region of interest was divided into two halves: the first half was used for the Al_2O_3NPs assay, while the second half was used to assess oxidative stress.

2.4 Nano-Alumina Assay

All reagents used were 99.9% pure and were carefully screened for aluminum contamination. Water for solution preparation was sourced from a dedicated deionization unit equipped with five distinct resins. Additionally, all glassware samples underwent acid washing followed by rinsing with deionized water before conducting the measurements.

The concentrations of aluminum (Al) ions in the hippocampus, cortex, striatum, and midbrain regions were measured using an Agilent 7700 series Inductively Coupled Plasma Mass Spectrometer (ICP-MS) with an auto-sampler (Agilent Technologies, Germany), as previously described by Morsy et al. (2016). The analysis was performed with an RF power of 1500 W, reflected power of ≤ 1 W, carrier gas flow of 1.1 L/min, and detection limit of 0.001 ng. The instrument was calibrated using an external standard (Agilent calibration standard no. 8500-6940).

To estimate the concentration of Al ions, an accurate weight of the brain area was measured using a mixture of pure concentrated nitric acid (HNO_3) and hydrogen peroxide (H_2O_2). The process involved pre-digesting the definite weight of a brain area in a Falcon tube for 5 h at room temperature, along with 5 ml of ultrapure HNO_3. The mixture was then transferred to a Teflon digestion vessel, and 1 ml of H_2O_2 was added. The digestion process was carried out using an Ethos Easy microwave system (Milestone, Italy), following the digestion program: power at 1200 W (100%), ramp time of 15 min, temperature set at 200°C, hold time of 15 min, and cooling time of 15 min.

After digestion, 5 ml of hydrochloric acid was promptly introduced to promote the formation of soluble aluminum complexes and inhibit the development of insoluble aluminum salts. Subsequently, the prepared samples were diluted with 10 ml of Milli-Q water and filtered through a Millipore membrane (0.45 m). This process rendered each sample ready for measurement. The concentration of aluminum ions in the tissues was quantified as micrograms per gram of dry weight (µg/g dry wt.).

2.5 Estimation of Glutathione

To estimate the levels of GSH in the brain, a significant weight of each brain area was homogenized and subsequently diluted with a 1:1 ratio of 4% sulfosalicylic acid (SSA). The mixture was then centrifuged at 5000 rpm for 10 min, passed through a Sep-Pak cartridge, and stored at -20°C for subsequent analysis.

High-performance liquid chromatography (HPLC) was used to determine the levels of glutathione (GSH), following the method outlined by [19]. GSH reference standards were prepared by dissolving the standards in 75% methanol at a concentration of 1 mg/ml. These standards were then diluted with the mobile phase buffer and injected into an HPLC Agilent 1200 system. The column employed was a Synergy 4 µm Hydro-RP 80A HPLC column, measuring 150 x 3.9 mm. The flow rate of 2 ml/min was maintained at a wavelength of 210 nm. The mobile phase consisted of potassium phosphate buffer (50 mM) at pH 2.7, along acetonitrile in a ratio of 97:3 (V/V) as the isocratic mobile phase. The retention times and concentrations of the injected GSH samples were automatically compared and matched with their corresponding standards from the working standard curve to determine the GSH concentrations in the samples. The concentrations of free GSH in the brain were expressed as micromols per gram of brain area (µmol/g tissue).

2.6 Estimation of Malondialdehyde

A significant weight of each brain area was homogenized and then the homogenate was diluted in a ratio of 1:2.75 with 0.1 M perchloric acid, centrifuged at 5000 rpm for 10 min, passed through a Sep-Pak cartridge, and stored at -20°C for further analysis. Standard preparation was performed according to [20] by dissolving 25 µl 1,1,3,3 tetraethoxypropane (TEP) in 100 ml of water to obtain a 1 mM stock solution. The working standard was prepared by the hydrolysis of 1 ml TEP stock solution in 50 ml 1% sulfuric acid and incubation for two hours at room temperature. The resulting MDA standard of 20 nmol/ml was further diluted with 1% sulfuric acid to yield the final concentration of 1.25 nmol/ml to get the standard for estimating total MDA.

The MDA samples were analyzed using an Agilent HP 1200 series. The analytical column used was a Supelcosil C18 with a particle size of 5 µm and a pore size of 80 A0 (250 × 4.6 ID). The mobile phase consisted of 30 mmol KH_2PO_4 and methanol (65%-35%, H2PO4 at pH 4), and the mobile phase was pumped at a flow rate of 1.5 ml/min. The wavelength used for detection was 250 nm following the method described by [21]. The HPLC chromatogram, retention time, and concentrations of the injected MDA samples were automatically compared to the corresponding standards of the working standard curve to determine the concentrations of MDA in the samples. The concentration of free MDA in brain tissue was expressed as micrograms per gram of brain tissue (µg/g tissue).

2.7 Statistical Analysis

The data in this study were found to follow a normal distribution, as confirmed by the Kolmogorov-Smirnov test. Therefore, parametric analysis was conducted. Specifically, a parametric multi-way analysis of variance (MANOVA) was conducted to investigate the impact of several independent variables (factors) on dependent variables (parameters). The independent variables included the experimental periods (3, 7, and 14 days), dosages of nano-alumina (0.00 and 0.96 g/kg every other day), and brain areas (the hippocampus, cortex, striatum, and midbrain). In addition, interactions between these variables were examined. The dependent variables of interest were the bioaccumulation of Al ions and the levels of MDA and GSH in the brains of the male rats. Post-hoc Tukey and Games-Howell tests were used to compare the two desired variables. Regression analysis and correlation coefficients were employed to investigate the relationships between various desired variables. The data presented in this study are expressed as mean ± standard error of the mean (SEM). Statistical analyses were performed using IBM SPSS Statistics (Statistical Package for the Social Sciences, version 29).

3. Results

Multivariate analysis of variance (MANOVA) was conducted to examine the impact of brain areas (BA: Hippocampus, cortex, striatum, and midbrain), experimental period (EP:3, 7, and 14 days), nano-alumina dose (D:0.00 and 0.96 mg/kg), and their interactions on the levels of aluminum ion (Al+3) bioaccumulation, glutathione (GSH), and malondialdehyde (MDA). The results indicate that all variables except MDA were significantly influenced by the factors under investigation (Table 1). Specifically, the main effects of BA, EP, and D as well as the interactions of BA*EP, BA*D, and EP*D were found to be significant. However, the three-way interaction between BA, EP, and D did not have a significant effect on MDA levels.

Table 1: Multivariate analysis of variance (MANOVA) examining the impact of brain areas (BA: Hippocampus, Cortex, Striatum, and Midbrain), experimental periods (EP: 3, 7, and 14 days), nano-alumina doses (D: 0.00 and 0.96 mg/kg), and their interactions on the levels of Al+3 ions (µg/g dry wt.), glutathione (GSH; mg/g), and malondialdehyde (MDA; mg/g).

Independent Variable	Dependent Variable	Sum of Squares	df	Mean Squares	F-calculated	Significant levels
BA	Al ions	210.698	3	70.233	537.875	P<0.0001
	GSH	9.062	3	3.021	148.510	P<0.0001
	MDA	154.226	3	51.409	56.027	P<0.0001
EP	Al ions	49.579	2	24.789	189.848	P<0.0001
	GSH	4.723	2	2.362	116.108	P<0.0001
	MDA	78.972	2	39.486	43.033	P<0.0001
D	Al ions	1434.045	1	1434.045	10982.585	P<0.0001
	GSH	32.565	1	32.565	1601.003	P<0.0001
	MDA	808.898	1	808.898	881.565	P<0.0001
BA*EP	Al ions	8.533	6	1.422	10.892	P<0.0001
	GSH	1.325	6	0.221	10.857	P<0.0001
	MDA	9.101	6	1.517	1.653	P≥0.05

BA*D	Al ions	170.774	3	56.925	435.955	P<0.0001
	GSH	8.739	3	2.913	143.216	P<0.0001
	MDA	10.333	3	3.444	3.754	P<0.01
EP*D	Al ions	50.363	2	25.182	192.853	P<0.0001
	GSH	5.686	2	2.843	139.778	P<0.0001
	MDA	71.353	2	35.676	38.881	P<0.0001
BA*EP*D	Al ions	7.931	6	1.322	10.123	P<0.0001
	GSH	1.101	6	0.184	9.022	P<0.0001
	MDA	6.271	6	1.045	1.139	P≥0.05
Error	Al ions	12.535	96	0.131		
	GSH	1.953	96	0.020		
	MDA	88.087	96	88.087		

df: indicates the degree of freedom.

The P-value of ≥0.05 indicates a non-significant effect.

P-values <0.0001, <0.01, and <0.05 indicates a significant effect at α=0.0001, 0.01, and 0.05 respectively.

According to the regression and correlation coefficient analyses, there were significant linear direct relationships between the accumulation of Al^{+3} ions in the hippocampus and cortex brain areas of rats in group II and the experimental periods. These relationships were accompanied by a significant positive correlation value of +0.99 (Table 2). Additionally, the experimental periods showed significant direct logarithmic relationships with the levels of Al+3 ions accumulated in the striatum and midbrain of these rats, with significant correlation coefficients of +0.97 and +0.99, respectively (Table 2). Post-hoc Scheffe's test revealed that in group II, the accumulation of Al^{+3} ions in the hippocampus, cortex, striatum, and midbrain after 14 days was significantly greater than that after 7 and 3 days, with the highest average observed after 14 days and the lowest after 3 days (Table 2). In contrast, in rats in group 1, there was no observed relationship between the experimental period and the Al^{+3} ion content in the studied brain areas. There was no notable effect of these periods on Al^{+3} content, indicating no differences between the Al^{+3} content of each studied brain area at any of the studied periods (Table 2).

After 3, 7, and 14 days, the cortical and striatal Al^{+3} ion contents in group I rats were found to be similar, but significantly higher than those in the hippocampus. The midbrain had the next highest levels of Al^{+3} ions (Table 2). In group II, there were no significant differences in the accumulation of Al^{+3} ions between the hippocampus and cortex at any of the experimental periods (3, 7, and 14 days). However, both regions showed significantly higher levels than the striatum, followed by the midbrain (Table 2). In all brain areas studied in group II, the accumulation of Al^{+3} ions was highest after 14 days, followed by 7 days, and then 3 days of instillation, as shown in Table 2.

According to the multivariate post-hoc multiple comparison tests, there were no significant differences in the average levels of GSH and MDA in the hippocampus, cortex, striatum, and midbrain of Group I during the 3-, 7-, and 14-day experimental periods (Table 3). Additionally, no relationships or correlation coefficients were observed between the experimental period and GSH and MDA levels in any of the brain areas of the control rats.

As presented in Table 3, the levels of GSH in the hippocampus and striatum of rats in Group II displayed a significant inverse relationship with the duration of the experiment. Conversely, in the cortex and midbrain, they exhibited inverse linear relationships and were accompanied by notably negative correlation coefficients of -0.91, -0.85, -0.99, and -0.99, respectively. Consequently, the concentrations of GSH in all examined brain regions significantly declined over time, with the highest average observed after 3 days and the lowest average observed after 14 days of instillation. Specifically, the concentration of GSH after three days was greater than that after seven days, which was greater than that after 14 days (Table 3).

Table 2. Aluminum ion (Al^{+3}) concentrations (μg/g dry weight) in rat brain areas (hippocampus, cortex, striatum, and midbrain) after 3, 7, and 14 days of daily nasal instillation of 0.00 mg (Group I, control) or 0.95 mg (Group II, Al2O3-NPs treated rats) of nano-alumina per kilogram of body weight.

Sources	Experimental Periods			Regression and Correlation coefficient
	3 days	7 days	14 days	
Hippocampus				
Group I	1.77±0.213	1.77±0.113	1.76±0.115	----------
Group II	9.38±0.637*	11.27±0.832*■	14.37±0.884*■♦	y= 0.4524x+8.054, r= +0.99•
Cortex				
Group I	2.12±0.081	2.10±0.138	2.18±0.113	----------
Group II	9.15±0.079*	10.43±0.350*■A	12.64±0.505*■♦A	y= 0.3171x+8.203, r= +0.99•
Striatum				
Group I	2.37±0.217a	2.36±0.049a	2.260±0.127a	----------
Group II	5.59±0.504*AB	6.90±.0345*■AB	7.88±0.418*■♦AB	y= 1.489ln(x)+3.97, r= +0.97•
Mid-brain				
Group I	1.20±0.091abc	1.14±0.090abc	1.19±0.046abc	----------
Group II	4.91±0.100*ABC	5.92±0.304*■ABC	6.76±0.164*■♦ABC	y= 1.20ln(x)+3.589, r= +0.99•

→ Data represented as means ± SEM.

→ In the same column, superscript letters a, b, and c indicate significant differences (P<0.05) in comparison to group I in the hippocampus, cortex, and striatum, respectively.

→ In the same column, superscript letters A, B, and C indicate significant differences (P<0.05) in comparison to group II in the hippocampus, cortex, and striatum, respectively.

→ The symbol (*) indicates a significant difference (P<0.05) in comparison to the corresponding group I in the hippocampus, cortex, striatum, and midbrain.

→ In the same row, the symbols (■ and •) indicate significant differences (P<0.05) in comparison to group II after 3 and 7 days of instillation, respectively.

→ The letter (y) indicates the expected Al ion concentration at various instilled doses (x) of Al_2O_3-NPs.

→ The letter (r) indicates the correlation coefficient of the experimental periods and levels of Al in the brain areas.

→ The symbol (●) indicates a significant correlation coefficient.

During the same experimental period, GSH accumulation in the hippocampus, cortex, striatum, and midbrain of group II was significantly lower than that in group I during the corresponding period (Table 3). In addition, during the experimental period, GSH accumulation in the midbrain was significantly higher than in the hippocampus, striatum, and cortex (Table 3).

Table 3 demonstrates that in Group II, there was a significant direct power relationship between the experimental period and the level of MDA in the hippocampus. In contrast, the cortex, striatum, and midbrain show noticeable direct logarithmic relationships. These relationships were supported by the significant correlation coefficients of +0.99, +0.97, +0.97, and +0.93 respectively, (Table 3). Accordingly, the levels of MDA in all the studied brain areas after 3 days were significantly lower than those after 7 and 14 days. The lowest average was observed after 3 days, while the highest was observed after 14 days (Table 3). Throughout the experimental period, MDA levels in the hippocampus, cortex, striatum, and midbrain of Group II mice were significantly higher than those in Group I mice (Table 3).

Table 3. Levels of glutathione (GSH, mg/dl) and malondialdehyde (MDA, mg/g) in rat brain areas (hippocampus, cortex, striatum, and midbrain) after 3, 7, and 14 days of daily nasal instillation of 0.00 mg (Group I, control) or 0.95 mg (Group II, Al2O3-NPs treated rats) of nano-alumina per kilogram of body weight.

Sources	Experimental Periods			Regression and Correlation coefficient
	3 days	7 days	14 days	
GSH				
Hippocampus				
Group I	3.78±0.097	3.90±0.154	3.93±0.146	----------
Group II	3.53±0.308*	3.06±0.083*■	2.90±0.043*■	y= $4.026x^{-0.129}$, r= -0.91•
Cortex				
Group I	3.92±0.098	3.95±0.138	3.98±0.124	----------
Group II	2.60±0.121*A	2.28±0.199*■A	1.84±0.044*■♦A	y= -0.068x+2.7871, r= -0.99•
Striatum				
Group I	3.86±0.195	3.94±0.131	3.84±0.148	----------
Group II	3.44±0.0208*B	2.10±0.088*■AB	1.91±0.032*■♦A	y= $5.015x^{-0.389}$, r= -0.85•
Mid-brain				
Group I	3.96±0.103	3.99±0.126	3.92±0.148	----------
Group II	4.11±0.091ABC	3.74±0.140*■ABC	2.99±0.158*■♦BC	y= -0.1024x+4.433, r= -0.99•
MDA				
Hippocampus				
Group I	7.78±1.085	8.57±1.540	8.03±0.610	----------
Group II	11.04±0.878*	12.99±0.718*■	14.87±0.985*■♦	y= $8.925x^{0.1933}$, r= +0.99•
Cortex				
Group I	8.92±0.983	7.95±0.978	8.59±0.721	----------
Group II	12.07±1.010*	14.76±0.739*■A	16.73±1.077*■♦A	y= 3.03ln(x)+8.78, r=+0.97•
Striatum				
Group I	7.61±1.277ab	8.20±0.502	7.14±1.011b	----------
Group II	11.46±0.512*	12.98±0.585*■B	14.08±0.716*■♦B	y=1.70ln(x)+9.61, r= +0.97•
Mid-brain				
Group I	5.75±0.653abx	5.97±0.782abc	6.76±0.529ab	----------
Group II	8.09±0.885*ABC	11.12±0.836*■ABC	12.39±2.007*■♦ABC	y= 2.82ln(x)+5.19, r=+0.93•

→ Data represented as means ± SEM.

→ In the same column, superscript letters a, b, and c indicate significant differences (P<0.05) in comparison to group I in the hippocampus, cortex, and striatum, respectively.

→ In the same column, superscript letters A, B, and C indicate significant differences (P<0.05) in comparison to group II in the hippocampus, cortex, and striatum, respectively.

→ The symbol (*) indicates a significant difference (P<0.05) in comparison to the corresponding group I in the hippocampus, cortex, striatum, and midbrain.

→ In the same row, the symbols (■ and •) indicate significant differences (P<0.05) in comparison to group II after 3 and 7 days of instillation, respectively.

→ The letter (y) indicates the expected Al ion concentration at various instilled doses (x) of Al_2O_3-NPs.

→ The letter (r) indicates the correlation coefficient of the experimental periods and levels of Al in the brain areas.

→ The symbol (●) indicates a significant correlation coefficient.

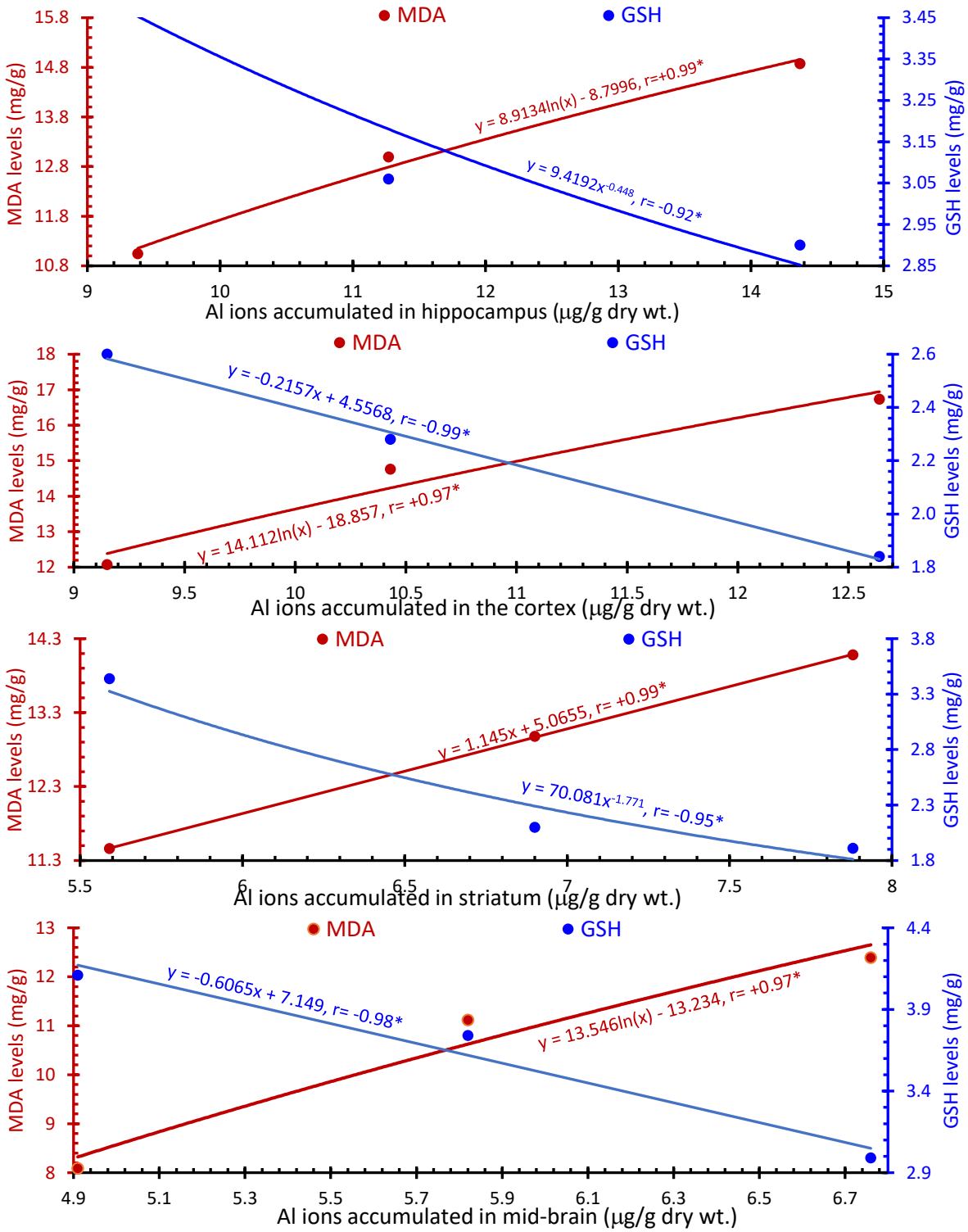

Figure 1: Relationships between the accumulation of aluminum (Al) ions in the hippocampus, cortex, striatum, and midbrain, and the levels of glutathione (GSH, mg/g) and malondialdehyde (MDA, mg/g) in the corresponding brain areas. The levels of Al ions are represented by x, while y represents the levels of GSH or MDA.

Figure 1 depicts the levels of Al^{+3} ions in the hippocampus and striatum, showing significant inverse power relationships with GSH levels. Conversely, the cortex and midbrain demonstrated notable inverse linear relationships, with correlation coefficients of -0.92, -0.95, -0.99, and -0.98. In contrast, the concentrations of Al^{+3} ions exhibit significant direct logarithmic relationships with the levels of MDA in the hippocampus, cortex, and midbrain. However, there was a significant direct linear relationship between the Al^{+3} ion concentration and MDA accumulation in the striatum, with correlation coefficients of +0.99, +0.97, +0.99, and +0.97, respectively (Figure 1).

4. Discussion

The present findings revealed that rats intranasally instilled with sublethal doses (0.94 g/kg) of Al_2O_3-NPs every other day exhibited notably elevated levels of Al ions in their hippocampus, cortex, striatum, and midbrain throughout all experimental time when compared with the corresponding control rats. It is noteworthy that the accumulation of Al ions in the brain regions was time dependent.

Following intranasal instillation with Al_2O_3-NPs, in the current work, aluminum (Al) can reach the brain via choroid plexuses or blood-brain barrier (BBB) absorption into olfactory neurons and then directly transfer into the brain [22]. The choroid plexus in the four cerebral ventricles synthesizes most of the cerebrospinal fluid (CSF) that fills the brain ventricles and the subarachnoid space surrounding the brain. The surface area of the 400 miles of brain capillaries that are the site of the BBB is approximately 12 m^2, which is approximately 1,000-fold that of the choroid plexuses. Visual examination of electron micrographs suggests that no cells in the brain are >30–40 μm from the nearest micro-vessel (BBB site) [23]. Thus, there is a much greater opportunity for rapid exchange between the blood and brain through the BBB than through the choroid plexuses and CSF compartment. Physiologically, intranasally instilled Al_2O_3-NPs can cross the blood-brain barrier (BBB) via multiple mechanisms, such as adsorptive-mediated transcytosis, receptor-mediated transcytosis, carrier-mediated transport, and passive diffusion [24, 25]. In adsorptive-mediated transcytosis, the nanoparticle surface charge interacts with the negatively charged cellular components of the tight junctions of the BBB [26]. The receptor-mediated transcytosis mechanism (RMT) is the principal pathway for the transport of aluminum by competition with macromolecules that are essential for the proper functioning of the brain across the BBB [27]. Therefore, Al_2O_3-NPs penetration across the BBB and accumulation in the hippocampus, cortex, striatum, and midbrain could be attributed to their physicochemical properties, such as polar surface area, nano-sized surface area, zeta potential, and lipophilicity (hydrogen bonding potential), providing the opportunity to estimate the permeability rates of Al_2O_3-NPs and their complexes across the rat's BBB from their octanol/buffer partitioning coefficient and nanosized particles [28].

In the current study, the sizes of nano-alumina (≤ 9 nm) were smaller than 20 nm and could easily cross the BBB [29]. Furthermore, the size of nanoparticles can also influence their biodistribution and clearance [30]. Additionally, nanosized particles tend to accumulate more readily in brain tissue and have a longer residence time in the brain than larger nanoparticles [29]. This is because smaller particles can diffuse more easily through the brain interstitium and therefore have a higher chance of interacting with brain cells owing to their low negative charge.

According to the current findings, the high polar surface-area-to-volume ratio of Al_2O_3-NPs exposes a large number of atoms or molecules to the surrounding environment, resulting in increased reactivity, that is, the surface area of nano-alumina is highly reactive, and has the ability to autoionize, and produces excessive levels of ions and reactive species that facilitate their interaction with brain regions, resulting in their high accumulation in the CNS and induction of oxidative stress [31]. Furthermore, the higher surface-area-to-volume ratio of Al_2O_3 nanoparticles allows for stronger interactions with other substances, allowing for more efficient adsorption and desorption processes, resulting in increased interaction with brain areas and, as a result, increased bioaccumulation, as demonstrated by our data. The highly enhanced surface reactions of Al_2O_3-NPs, as observed in our findings, promote surface reactions such as oxidation, reduction, and catalysis, resulting in improved efficiency in various chemical processes and their accumulation in brain areas, i.e., the larger surface area of nanoparticles provides more active sites for catalytic reactions, resulting in enhanced efficiency and selectivity and their accumulation in the studied brain areas [32].

On the other hand, the zeta potential of nanoparticles, which refers to their surface charge, is also an important factor affecting their interactions with the BBB. Nanoparticles with a low zeta potential (negatively charged nanoparticles), as in the current findings, can improve brain uptake owing to the electrostatic attraction to the positive charges of the BBB and increasing nano-alumina accumulation [32]. However, nanoparticles with a high zeta potential may be repelled by the highly negative charges of the BBB.

Our present results indicate that the highest accumulation of Al2O3NPs is observed in the hippocampus, followed by the cortex, striatum, and midbrain. This can be attributed to the significant thickness of tight junctions (TJs) in the blood-brain barrier (BBB) surrounding the midbrain, followed by the striatum, cortex, and ultimately the hippocampus. The blood-brain barrier (BBB) is composed of tight junctions (TJs), which are proteins located at the boundaries of epithelial and endothelial cells in various regions of the brain [34]. These junctions play a crucial role in maintaining cellular connectivity. TJs consist of transmembrane proteins such as occludin and claudins, junctional adhesion molecules (JAMs), zona occludens (ZOs), and cytoskeletal protein F-actin [35]. Bioaccumulation of Al_2O_3NPs and their invasion of the brain areas caused abnormal expression of proteins associated with TJs, leading to the destruction of TJs, structural damage, and dysfunction of endothelial and epithelial cells [36]. These factors have been linked to the development and progression of various diseases. Stroke is characterized by damage to and dysfunction of the blood-brain barrier (BBB). TJs are directly involved in the maintenance of BBB integrity. Multiple regulatory mechanisms of phosphorylation, matrix metalloproteinases (MMPs), and microRNAs control the expression of TJ-related proteins and influence BBB permeability, which is highly disturbed by Al ion accumulation [37].

Lipophilicity is the ability of a substance to dissolve in lipids (in nonpolar solvents). Al_2O_3-NPs, in the present work, were highly lipophilic and this property gave these nanoparticles a better chance of crossing the BBB than hydrophilic nanoparticles [38]. Lipophilic substances have an affinity for the lipid bilayer membranes of BBB cells, allowing them to easily partition into lipids and pass through the BBB [39].

Kinetically, the brain elimination half-life time (t1/2) of bulk alumina in rats has been estimated to range from 0.7 to 9 years [40]. Conversely, the elimination time of Al_2O_3NPs was found to be 12.7 years [41]. The extended elimination time of nanoparticles demonstrates their exceptional ability to infiltrate tissues and accumulate within membranes, intracellular compartments, and organelles. Several studies [42] have indicated that the large surface area of Al_2O_3NPs generates a high voltage on the outer surface, thereby promoting the release of free electrons and reactive oxygen species (ROS) from Al_2O_3-NPs. These ROS can easily cross the blood-brain barrier (BBB), leading to significant oxidative damage and the destruction of cell membranes [43]. [44] observed that exposure to aluminum oxide nanoparticles (Al_2O_3NPs) disrupts the integrity of endothelial cells in both neural and non-neural tissues. The authors attribute this to the strong ability of Al_2O_3NPs to modify cerebral blood vessels, disrupt the potential of mitochondrial membranes, induce oxidative stress in cells, and decrease the expression of tight junction proteins in brain endothelial cells. These effects ultimately result in reduced BBB efficiency [45]. These findings align with another study that demonstrated how nanoparticles easily enter cell membranes, accumulate in the cytoplasm, disrupt cellular metabolism, and cause various cellular dysfunctions, including cell death [46]. Most of the Al ions circulating in the blood are eliminated by the kidneys (approximately 95%) through urine, potentially as Al citrate [47].

The brain is more susceptible to oxidative stress because of its poor antioxidant content, high oxidizable polyunsaturated fatty acids and iron content, and high metabolic rate (48). Herein, we recorded a significant elevation in brain MDA and depletion of GSH in the brain areas of Al_2O_3-NPs administered to rats. Consistent with our results, [49] showed that excessive generation of ROS with consequent oxidative stress is the major mechanism of nanoparticle-induced toxicity due to the large surface area, compared to their larger counterparts. Similar to our results, Al_2O_3-NPs administered orally to rats have been shown to increase lipid peroxidation and deplete GSH levels in the brain [50, 51].

Oxidative stress in the brain has been reported in rats that received nanoparticles intraperitoneal, intravenous, or via intranasal instillation [52]. The elevated level of MDA with GSH depletion indicated a redox imbalance. MDA, a lipid peroxidation (LPO) marker, is a toxic adduct that contributes to neuronal cell death [53]. Low GSH levels

could be attributed to excessive utilization of scavenging ROS as a response to the detoxification of H_2O_2, superoxide radicals, and superoxide radicals by catalase (CAT) and superoxide dismutase (SOD) [54]. The increased utilization of GSH by glutathione transferase (GST) enzymes may contribute to GSH depletion. In agreement with our findings, [55] reported a significant decrease in GSH levels as a direct response to nano-alumina administration.

Our current data show that the levels of glutathione (GSH) in the hippocampus, cortex, striatum, and midbrain of rats in group II (given Al_2O_3NPs) were significantly lower than those in group I (control) at 3, 7, and 14-day time points. In contrast, MDA concentrations were significantly higher in Group II. Furthermore, the duration of the experiment demonstrated an apparent inverse relationship with GSH levels, as indicated by the significant negative correlation coefficient. In contrast, MDA levels exhibited a significantly positive correlation coefficient, suggesting a direct relationship.

The antioxidant defense system is supported by glutathione reductase (GR), a flavoprotein that converts glutathione disulfide (GSSG) from its oxidized form to its reduced form (GSH) [56]. GR contains a disulfide bond in its active site, and the presence of free Al ions may interfere with and compete for this site, thereby inhibiting and/or blocking GR activity [57]. This interference can reduce the conversion of GSSG to GSH, making cells more susceptible to oxidative damage and causing significant depletion of GSH levels and an increase in GSSG. Additionally, GSH plays a protective role against oxidative stress, and its alteration causes a significant abnormal oxidative state [58]. However, as oxidative stress persists and tissue protein levels decrease owing to total protein oxidation caused by Al [59, GSH synthesis is unable to meet the demand, leading to GSH depletion [60]. Previous studies [61; 62; 63] have also shown that micro- and nanosized Cd and Al can deplete GSH in tissues.

[64] found that high doses of Al can reduce GSH synthesis by increasing the production of oxidative free radicals and decreasing glutathione synthase activity. The current study further supports the toxicity of Al_2O_3NPs by demonstrating a significant inverse relationship between the levels of accumulated Al ions in various brain regions (hippocampus, cortex, striatum, and midbrain) and GSH concentrations. This suggests that the decreased antioxidant status of the cells is primarily responsible for the observed toxicity of Al_2O_3NPs.

The levels of MDA in the brain areas of rats exposed to Al_2O_3NPs were significantly increased, indicating lipid peroxidation (LPO) and oxidative damage [65]. The concentration of MDA varied in different brain regions and was influenced by time and brain area, suggesting that the instilled Al_2O_3NPs may have generated reactive free radicals that initiated LPO. This suggests that experimental rats experienced severe oxidative stress [66]. The toxicity of Al2O3NPs can be attributed to the abnormally high accumulation of Al ions, as mentioned above, which interact with the intracellular organelles of neurons and induce excessive release of reactive oxygen species (ROS) from their hyperactive surface [67]. As a result, Al_2O_3NPs can cause toxicity by directly interacting with cell organelles and forming chemical compounds with DNA, RNA, and proteins. The Al ions released from the outer surface of Al_2O_3NPs chemically interact with iron in different tissues, resulting in the liberation of redox-active free iron [68].

[69] conducted a study showing that the levels of thiobarbituric acid reactive substances (TBARS), which indicate lipid peroxidation (LPO), significantly increase in various brain areas when exposed to aluminum ions. This finding supports a previous report by [70], who demonstrated that iron ions (Fe^{2+}) are potent initiators of lipid peroxidation in the brain, resulting in a significant increase in malondialdehyde (MDA) content.

The increase in LPO observed in the presence of Fe2+ can be attributed to the ability of Fe^{2+} to catalyze electron transfer reactions that generate reactive oxygen species (ROS), including the highly reactive hydroxyl radical (OH•). This hydroxyl radical is formed via Fenton's reaction, in which hydrogen peroxide (H_2O_2) reacts with Fe^{2+}. Furthermore, iron ions can break down lipid peroxides, leading to the formation of peroxyl and alkoxyl radicals, which further promotes the propagation of lipid peroxidation [71]. The ionic radius of Al^{3+} closely resembles that of Fe^{3+}, suggesting that Al^{3+} may occupy Fe^{3+} sites. Al ions can bind to the iron-carrying protein transferrin, reducing the binding of Fe^{3+} [72]. This increase in free intracellular Fe^{3+} leads to peroxidation of membrane lipids and subsequent membrane damage. [71] reported a 5.6 times higher amount of Al in ferritin extracted from Alzheimer's disease compared to matched control samples. Enzymatically, the current significant overproduction of MDA as a response to LPO oxidative damage in the studied brain areas of rats exposed to Al_2O_3NPs may be attributed to the significant decrease in the activities of antioxidant enzymes superoxide dismutase (SOD), catalase (CAT), and

glutathione peroxidase (GPx) [54]. This leads to an increased generation of reactive oxygen species (ROS), which can attack the double bonds in membrane lipids and cause a significant increase in lipid peroxidation and, in turn, MDA. Additionally, lipid peroxidation promotes mitochondrial respiration, which is a major source of ROS, thereby exacerbating oxidative stress-induced metal toxicity [73].

For instance, when nano-titanium dioxide (TiO_2-NPs) was injected into the abdominal cavity of mice, it resulted in a significant increase in lipid peroxidation (LPO), significant decreases in glutathione (GSH) levels, and an alteration in the activity of antioxidant enzymes as well as marked depletion in levels of MDA, all of which were dose- and time-dependent [74].

References

[1]. K. Gajanan, S.N. Tijare, Applications of nanomaterials, Mater. Today Proc. 5 (2018) 1093–1096.

[2]. Y.K. Huang, Recent Developments in Food Packaging Based on Nanomaterials, in: Nanomaterials, 8, Basel, Switzerland, 2018, p. 10.

[3]. H. Liu, Y. Yang, Y. Liu, J. Pan, J. Wang, F. Man, W. Zhang, G. Liu, Melanin-like nanomaterials for advanced biomedical applications: a versatile platform with extraordinary promise, Adv. Sci. 7 (7) (2020), 1903129

[4]. X. Pan, J. Ji, N. Zhang, M. Xing, Research progress of graphene-based nanomaterials for the environmental remediation, Chin. Chem. Lett. 31 (6) (2020) 1462–1473

[5]. E. Rajasekaran, M. Govindhan, Two-dimensional earth-abundant transition metal oxides nanomaterials: synthesis and application in electrochemical oxygen evolution reaction, Langmuir: ACS J. Surf. Colloids 36 (17) (2020) 4728–4736

[6]. V. Kumar, K.D. Gill, Oxidative stress and mitochondrial dysfunction in aluminium- neurotoxicity and its amelioration: a review, Neurotoxicology 41 (2014) 154–166.

[7]. W. Dai, R.D. Nadadur, J.A. Brennan, H.L. Smith, K.M. Shen, M. Gadek, C.R. Weber, ZO-1 regulates intercalated disc composition and atrioventricular node conduction", Circ. Res. 127 (2) (2020) e28–e43.

[8]. Behzadi, Shahed et al. "Cellular uptake of nanoparticles: journey inside the cell." Chemical Society reviews vol. 46,14 (2017): 4218-4244. doi:10.1039/c6cs00636a

[9]. Chou, L. Y., Ming, K., & Chan, W. C. (2011). Strategies for the intracellular delivery of nanoparticles. Chemical Society reviews, 40(1), 233–245. https://doi.org/10.1039/c0cs00003e

[10]. Manke, Amruta et al. "Mechanisms of nanoparticle-induced oxidative stress and toxicity." BioMed research international vol. 2013 (2013): 942916. doi:10.1155/2013/942916

[11]. Ju-Nam, Y., & Lead, J. R. (2008). Manufactured nanoparticles: an overview of their chemistry, interactions and potential environmental implications. The Science of the total environment, 400(1-3), 396–414. https://doi.org/10.1016/j.scitotenv.2008.06.042

[12]. D. Ge, Q. Du, B. Ran, X. Liu, X. Wang, X. Ma, F. Cheng, B. Sun, The neurotoxicity induced by engineered nanomaterials, Int. J. Nanomed. 14 (2019) 4167–4186.

[13]. O.A. Hussein, A.M.M. Abdel-Hafez, A. Kareim, Abd El, Rat hippocampal CA3 neuronal injury induced by limb ischemia/reperfusion: a possible restorative effect of alpha lipoic acid, Ultrastruct. Pathol. 42 (2) (2018) 133–154.

[14]. Luo, Y. H., Chang, L. W., & Lin, P. (2015). Metal-Based Nanoparticles and the Immune System: Activation, Inflammation, and Potential Applications. BioMed research international, 2015, 143720. https://doi.org/10.1155/2015/143720

[15]. J.H. Jhoo, H.C. Kim, T. Nabeshima, K. Yamada, E.J. Shin, W.K. Jhoo, J.I. Woo, Beta-amyloid (1-42)-induced learning and memory deficits in mice: involvement of oxidative burdens in the hippocampus and cerebral cortex", Behav. Brain Res. 155 (2) (2004) 185–196.

[16]. H. Jiao, Z. Wang, Y. Liu, P. Wang, Y. Xue, Specific role of tight junction proteins claudin-5, occludin, and ZO-1 of the blood-brain barrier in a focal cerebral ischemic insult, J. Mol. Neurosci. 44 (2) (2011) 130–139.

[17]. Zhang, Q.; Ding, Y.; He, K.; Li, H.; Gao, F.; Moehling, T. J.; Wu, X.; Duncan, J. and Niu, Q. (2018): Exposure to alumina nanoparticles in female mice during pregnancy induces neurodevelopmental toxicity in the offspring. Frontiers in pharmacology, 9, 253.

[18]. A Ashok, SS Andrabi, S Mansoor, Y Kuang, BK Kwon, V Labhasetwar (2022): Antioxidant therapy in oxidative stress-induced neurodegenerative diseases: Role of nanoparticle-based drug delivery systems in clinical translation. ntioxidants, 11(2), 408; https://doi.org/10.3390/antiox11020408.

[19]. Jayatilleke, E. and Shaw, S. (1993). A high performance liquid chromatographic assay for reduced and oxidized glutathione in biological samples. Anal. Biochem., 214(2): 452-457.

[20]. Karatepe, M. (2004). Simulatenous determination of ascorbic acid and free malondialdehyde in human serum by HPLC-UV. Chromatographic Line., 12:362-365.

[21]. Karalas, F.; Karatepe, M. and Baysar, A. (2002). Determination of free malondialdehyde in human serum by high performance liquid chromatography. Anal. Biochem., 311:76-79.

[22]. Manju Pandey (2022): Nose-to-Brain Targeted Drug Delivery Bypassing the Blood-Brain Barrier: An Overview. Advancements in Controlled Drug Delivery Systems, 1-25. DOI: 10.4018/978-1-7998-8908-3.ch007

[23]. Bhupesh Sharma, Kanishk Luhach, G.T. Kulkarni (2019): 4 - In vitro and in vivo models of BBB to evaluate brain targeting drug delivery. A Focus on Nanotechnology and Nanoparticulates 2019, Pages 53-101

[24]. Yingchao Han, Huifang Zhang, Jingsi Zhang, Yanni Wang, Yue Zhou, Huan Li, Qinli Zhang, Qiao Niu (2022): A study on cognitive impairment of mice exposed to nano-alumina particles by nasal drip. Journal of Trace Elements in Medicine and Biology, 73: 127003.

[25]. S Ding, AI Khan, X Cai, Y Song, Z Lyu, D Du, P Dutta, Yuehe Lin (2020): Overcoming blood–brain barrier transport: Advances in nanoparticle-based drug delivery strategies. Materials today, Volume 37, Pages 112-125.

[26]. Fruzsina R. Waltera,b, Ana R. Santa-Mariaa,c, Mária Mészárosa, Szilvia Veszelkaa, András Déra, and Mária A. Deli (2021): Surface charge, glycocalyx, and blood-brain barrier function. Tissue Barriers, 9(3), e1904773 (23 pages).

[27]. TM Sim, D Tarini, ST Dheen, BH Bay, DK Srinivasan (2020): Nanoparticle-Based Technology Approaches to the Management of Neurological Disorders. Int. J. Mol. Sci., 21(17), 6070; https://doi.org/10.3390/ijms21176070.

[28]. Gamal M Morsy, Kawther S Abou El-Ala and Atef A Ali (2016): Studies on fate and toxicity of nanoalumina in male albino rats: Lethality, bioaccumulation and genotoxicity. Toxicology and Industrial Health, 32(2) 344–359.

[29]. J Yuan, CC Nguyen, Y Mo, Y Zhang, Y Zhang, Q Zhang (2023): Neurotoxicity of Aluminum and Its Compound Nanoparticles. Neurotoxicity of Aluminum, pp 229–254.

[30]. GM Morsy (2014): Evaluation of toxicokinetic parameters of nanoalumina in serum and tissues of male albino rats. Egyptian Journal of Zoology, 4 (62), 93-110.

[31]. DM Brown, MR Wilson, W MacNee, V Stone, K. Donaldson (2001): Size-dependent proinflammatory effects of ultrafine polystyrene particles: a role for surface area and oxidative stress in the enhanced activity of ultra-fines. Toxicology and applied Pharmacology, 175(3): 191-199.

[32]. S Kango, S Kalia, A Celli, J Njuguna, Y Habibi, R Kumar (2013). Surface modification of inorganic nanoparticles for development of organic–inorganic nanocomposites—A review. Progress in Polymer Science, 38(8): 1232-1261.

[33]. G Karunakaran, R Suriyaprabha, V Rajendran, N Kannan (2015): Effect of contact angle, zeta potential and particles size on the in vitro studies of Al2 O3 and SiO2 nanoparticles. Nanobiotechnology, 9(1): 27-34.

[34]. S Zhang, P Gong, J Zhang, X Mao, Y Zhao, H Wang, L Gan, X Lin (2020): Specific frequency electroacupuncture stimulation transiently enhances the permeability of the blood-brain barrier and induces tight junction changes. Front. Neurosci., 14: 1-13.

[35]. X Zheng, B Ren, Y Gao (2023): Tight junction proteins related to blood-brain barrier and their regulatory signaling pathways in ischemic stroke. Biomedicine & Pharmacotherapy, vol 165.

[36]. S Ishaq, A Liaqat, A Hameed, T. Ahmed (2021): Biochemical mechanisms of aluminum and other metals exposure, their brain entry mechanisms, effects on blood brain barrier and important pharmacokinetic parameters in neurological disorders. Biochem. Mech. Alum, 1-32.

[37]. Y Zhao, L Gan, L Ren, Y Lin, C Ma, X Lin (2022): Factors influencing the blood-brain barrier permeability. Brain Research, 1788(1): Volume 1788, 1.

[38]. GM Morsy, BM Ahmed, AK hassan (2021): Relationship Between Bioaccumulation of Aluminum Oxide Nanoparticles and Some Elements in Male Rats at Acute Experiments. Alfarama Journal of Basic & Applied Sciences, 2(2): 224-238.

[39]. X Feng, Y Zhang, C Zhang et al. (2020): Nanomaterial-mediated autophagy: coexisting hazard and health benefits in biomedicine. Particle and Fibre Toxicology, volume 17(53).

[40]. K Wu, Y Sun, J Liu, J Xiong, J Wu, J Zhang, M Fu, et al. (2021): Nonthermal plasma catalysis for toluene decomposition over BaTiO3-based catalysts by Ce doping at A-sites: The role of surface-reactive oxygen species. Journal of Hazardous Materials, Volume 405, 124156.

[41]. CA Juan, JM Pérez de la Lastra, FJ Plou, E Pérez-Lebeña (2021): The chemistry of reactive oxygen species (ROS) revisited: outlining their role in biological macromolecules (DNA, lipids and proteins) and induced pathologies. Int. J. Mol. Sci. 2021, 22(9), 4642; https://doi.org/10.3390/ijms 22094 642.

[42]. Y Chen, L Dong, F Deng, Y Cao, et al. (2021): Integrated high-throughput small RNA and transcriptome sequencing unveil the shape-dependent toxicity of nano-alumina in rat astrocytes. Environmental Sciences Europe, volume 33(95).

[43]. P Xiong, X Huang, N Ye, Q Lu, G Zhang, et al.(2022): Cytotoxicity of Metal-Based Nanoparticles: From Mechanisms and Methods of Evaluation to Pathological Manifestations. Advanced Science, 9(16).

[44]. L Xuan, Z Ju, M Skonieczna, PK Zhou, R Huang, et al. (2023): Nanoparticles-induced potential toxicity on human health: Applications, toxicity mechanisms, and evaluation models. MedComm, Volume 4(4), e327.

[45]. IO Igbokwe, E Igwenagu, NA Igbokwe (2019): Aluminium toxicosis: a review of toxic actions and effects. Interdiscip Toxicol., 12(2): 45–70. doi: 10.2478/intox-2019-000.

[46]. S Demirci-Cekic, G Özkan, AN Avan, S Uzunboy (2022): Biomarkers of oxidative stress and antioxidant defense. Journal of Pharmaceutical and Biomedical Analysis, 209, 114477.

[47]. AB Sengul, E Asmatulu (2020): Toxicity of metal and metal oxide nanoparticles: A review. Environmental Chemistry Letters, 18:1659–1683.

[48]. A De, S Ghosh, M Chakrabarti, I Ghosh (2020): Effect of low-dose exposure of aluminium oxide nanoparticles in Swiss albino mice: Histopathological changes and oxidative damage. Toxicology and Industrial Health, 36(8): 121-126.

[49]. Z Hussain, HE Thu, I Elsayed, MAS Abourehab (2020): Nano-scaled materials may induce severe neurotoxicity upon chronic exposure to brain tissues: A critical appraisal and recent updates on predisposing factors…

[50]. Z Ferdous, A Nemmar (2020): Health impact of silver nanoparticles: a review of the biodistribution and toxicity following various routes of exposure. Int. J. Mol. Sci., 21(7): 2375; https://doi.org/10.3390/ijms21072375.

[51]. EG Canli, C Gumus, M Canli, HB Ila (2022): The effects of titanium nanoparticles on enzymatic and non-enzymatic biomarkers in female Wistar rats. Drug and Chemical Toxicology, 45(1): 233-245.

[52]. SS Ali, H Ahsan, MK Zia, T Siddiqui, F Halim Khan (2020): Understanding oxidants and antioxidants: Classical team with new players. Journal of Food Biochemistry, 44(3), e13145.

[53]. H Li, T Huang, Y Wang, B Pan, L Zhang, Q Zhang, Q Niu (2020): Toxicity of alumina nanoparticles in the immune system of mice. Nanomedicine, 15(9): 127-135.

[54]. S Raj Rai, C Bhattacharyya, A Sarkar (2021): Glutathione: role in oxidative/nitrosative stress, antioxidant defense, and treatments. Chemistry Select, 6(18): 4566-4590.

[55]. Newairy AS, Salama AF, Hussien HM, Yousef MI. (2009). Propolis alleviates aluminum-induced lipid peroxidation and biochemical parameters in male rats. Food Chem Toxicol 47: 1093–1098.

[56]. NG Abdelhameed, YH Ahmed, NAE Yasin (2023): Effects of Aluminum Oxide Nanoparticles in the Cerebrum, Hippocampus, and Cerebellum of Male Wistar Rats and Potential Ameliorative Role of Melatonin. ACS Chem. Neurosci. 2023, 14, 3, 359–369.

[57]. Khan H, Khan MF, Khan BA, Razaque G, Haque N, Akhter B, et al. (2012): Evaluation of the interaction of aluminium metal with glutathione in human blood components. Biomedical Research 23(2): 237–240.

[58]. Karmakar R, Banik S, Bandyopadhyay S and Chatteqee M (1998) Cadmium-induced alterations of hepatic lipid peroxidation, glutathione S-transferase activity and reduced glutathione level and their possible correlation with chromosomal aberration in mice: a time course study. Mutation Research 397: 183–190.

[59]. Shrivastava S (2011) S-Allyl-cysteines reduce amelioration of aluminium induced toxicity in rats. American Journal of Biochemistry and Biotechnology 7(2): 74–83.

[60]. Li ZH, Li P and Randak T (2010) Effect of a human pharmaceutical carbamazepine on antioxidant responses in brain of a model teleost in vitro: an efficient approach to biomonitoring. Journal of Applied Toxicology 30: 644–648.

[61]. Morsy, G. M.; Abou El-Ala, K. S. and Ali, A. A. (2016a): Studies on fate and toxicity of nanoalumina in male albino rats: oxidative stress in the brain, liver and kidney. Toxicology and industrial health, 32(2): 200-214.

[62]. Orihuela D, Meichtry V, Pregi N and Pizarro M (2005): Short-term oral exposure to aluminium decreases glutathione intestinal levels and changes enzyme activities involved in its metabolism. Journal of Inorganic Biochemistry 99: 1871–1878

[63]. Abdel-Wahab WM. (2012). AlCl3-induced toxicity and oxidative stress in liver of male rats: protection by melatonin. Life Sci J 9: 1173–1182.

[64]. Hamad HR (2012) Modulation of the genotoxic effect induced by titanium dioxide nanoparticles in mice (Mus musculus). PhD Thesis, Cairo University, Faculty of Science, Zoology Department, Egypt.

[65]. Chang YN, Zhang M, Xia L, Zhang J and Xing G (2012): The toxic effects and mechanisms of CuO and ZnO nanoparticles. Materials (5): 2850–2871.

[66]. Gutteridge JMC, Quinlan GJ, Clark I and Halliwell B (1985) Aluminium salts accelerate peroxidation of membrane lipids stimulated by iron salts. Biochimica et Biophysica Acta 835: 441–447.

[67]. Julka D, Gill KD (1996) Effect of aluminium on regional brain antioxidant defense status in Wistar rats. Research in Experimental Medicine 1996:187–194.

[68]. Oboh G, Puntel RL and Rocha JB (2007) Hot pepper (Capsicum annuum, tepin and Capsicum chinese, Habanero) prevents Fe2þ-induced lipid peroxidation in brain – in vitro. Food Chemistry 102: 178–185.

[69]. Zago MP, Verstraeten SV and Oteiza PI (2000) Zinc in the prevention of Fe2þ initiated lipid and protein oxidation. Biological Research 33(2): 143–150.

[70]. Nehru B, Anand P (2005) Oxidative damage following chronic aluminium exposure in adult and pup rat brains. Journal of Trace Elements in Medicine and Biology 19: 203–208.

[71]. F Liu, Z Zhang, L Zhang, RN Meng, J Gao (2022): Effect of metal ions on Alzheimer's disease. Brain and Behavior, 12(3) e2527.

[72]. GM Morsy, KS Abou El-Ala, Atef A Ali (2016): Studies on fate and toxicity of nanoalumina in male albino rats: Oxidative stress in the brain, liver and kidney. Toxicology and Industrial Health, 32(2): 200–214.

[73]. Juan, Celia Andrés et al. “The Chemistry of Reactive Oxygen Species (ROS) Revisited: Outlining Their Role in Biological Macromolecules (DNA, Lipids and Proteins) and Induced Pathologies.” International journal of molecular sciences vol. 22,9 4642. 28 Apr. 2021, doi:10.3390/ijms22094642.

[74]. Mailloux, Ryan J. “An Update on Mitochondrial Reactive Oxygen Species Production.” Antioxidants (Basel, Switzerland) vol. 9,6 472. 2 Jun. 2020, doi:10.3390/antiox9060472.